https://doi.org/10.12442/j.issn.1002-185X.20250613

# Effect of current density on the microstructure, corrosion resistance and wear resistance of micro-arc oxidation coatings on 2195 Al-Li alloy in a silicate-phosphate electrolyte solution

**Jin Zonghan, Feng Changjie, Zhang Yudi, Wu Hong, Wang Henan**

*School of Materials Science and Engineering, Shenyang Aerospace University, Shenyang110136, China;*

**Abstract**: Ceramic coatings were prepared on 2195 Al−Li alloy by micro-arc oxidation (MAO) in a silicate-phosphate electrolyte solution under different current densities. The effect of current density varying from 2 to 8 A/dm$^2$ on the microstructure, corrosion and wear behavior of the coatings were investigated. The surface and cross-sectional morphologies, composition and roughness of the MAO coatings were analyzed by scanning electron microscope (SEM), energy spectrometer (EDS), X-ray diffractometer (XRD), X-ray photoelectron spectroscopy (XPS) and surface roughness meter. The results show that with the increase of current density, the roughness and thickness of the MAO coating increase. The MAO coatings are mainly composed of γ-$Al_2O_3$ and a small amount of α-$Al_2O_3$. The MAO coatings prepared under the maximum current density is densest. Potentiodynamic polarization tests indicate that the corrosion resistance of coatings increase with the current density. When the current density is 8 A/dm², the MAO coating exhibits the best corrosion resistance, with a corrosion potential of -0.536 V and a corrosion current density of $4.32\times10^{-7}$ A/cm², which is two orders of magnitude lower than that of the substrate. Electrochemical Impedance Spectroscopy (EIS) results indicate that, at a current density of 8 A/dm², the sample possesses the largest capacitive arc radius and the highest impedance magnitude in the low-frequency region. The wear resistance of the MAO coatings increases with the current density. When the current density is 2 A/dm$^2$, the wear mechanism Mainly dominated by abrasive wear. Further increasing the current density, the wear mechanism transformed to abrasive wear. The MAO coatings prepared at 8 A/dm$^2$ show the best wear resistance with a wear rate of $0.1355\times10^{-3}$ mm$^3$/N·m.

**Keywords:** Al-Li alloy; micro-arc oxidation; microstructure; corrosion resistance; wear resistance

## 1. Introduction

Under the background of the continuous development of science and technology, the requirements for lightweight materials in the fields of automobile, ship, aviation, etc. are becoming more and more urgent. In addition, environmental problems such as carbon emissions from vehicles, aircraft and other means of transportation also guide people to choose quantities of lighter materials to lose weight and achieve the goal of reducing emissions. Aluminum lithium alloys have superior specific strength and specific elastic modulus, in which lithium is the lightest metal element and its density is only 0.53 g/cm$^3$, which is added to aluminum to form aluminum lithium alloy. Aluminum-lithium alloy has high specific strength and stiffness, good corrosion resistance, and excellent low-temperature fatigue performance[1]. Therefore, aluminum-lithium alloys have become one type of the best materials to replace the traditional aluminum alloys. However, the hardness of aluminum-lithium alloys are low, and the presence of amorphous and extremely thin natural oxide film on the surface makes their wear resistance and corrosion resistance weak, which limits their applications.

Micro-arc oxidation (MAO) is a relatively new efficient and environmentally friendly modification technology. Micro-arc discharge occurs on the sample surfaces during process of MAO with a series of complex reactions, such as electrochemical, thermochemical, plasma chemistry and high temperature phase transition, resulting in the formation of dense ceramic coatings[2-4], The thickness of the coatings ranges from tens to hundreds of micrometers, with excellent corrosion, wear, bionic, and thermal insulation properties. MAO is a promising technique in surface engineering because of its thick, dense and

Fundation Item: The financial support from the Liao Ning Revitalization Talents Program (Grant No.XLYC 2002031)
Corresponding author: Feng chanjie, Ph.D , Professor, School of Materials Science and engineering, Shenyang Aerospace University, Shenyang110136, China,
Author: Jin zonghan, M,S. School of Materials Science and engineering, Shenyang Aerospace University, Shenyang110136, China, E-mail: 13361359636@126.com

hard ceramic coatings on valve metals and their alloys[5-7]. The performance of MAO coatings is affected by many factors, such as electrolyte[8], electrochemical parameter[9,10] and power supply type[11]. KALKANCI[12] found the thickness of ceramic coating increased with the increase of current density in all solutions in a certain range. The higher the current density, the faster the growth rate of the coating. Xiang et al[13] investigated the microstructure and properties of the ceramic layer obtained after micro-arc oxidation of 6063 aluminum alloy with different current densities, and found that the pore density of the coating decreases with the increase of the current density, when the current density is 15 A/dm$^2$, the coating shows the best mechanical properties and the best corrosion resistance.

However, micro-arc oxidation still has many problems, such as MAO coatings often suffer from loose and porous surface due to the presence of discharge microholes, and some small cracks[14].In particular, the inhomogeneity of the arc discharge, as well as the subsequent rapid cooling and repetitive discharge, tends to lead to the inhomogeneous growth of the MAO coatings as well as the formation of porous structures.[15] This will lead to a decrease in the corrosion resistance of the oxidized alloy.

In recent years, many methods have been used for micro-arc oxidation to improve the corrosion resistance of the oxidized alloy, such as ultrasonic-assisted machining[15], and adding $SiO_2$ nanoparticles to the electrolyte[16].

However, There are few reports available on the effect of current density on the properties of MAO coatings[12,13], especially for Al-Li alloys. In the present study, MAO coatings have been prepared on 2195 Al-Li alloy by varying the current density using alkaline silicate-phosphate electrolyte. The prepared coatings have been characterized for their structure, morphology and roughness. The electrochemical corrosion behavior of the coatings has been studied by potentiodynamic polarization. The wear resistance and mechanism of the MAO coatings prepared at different current densities is also investigated.

## 2. Experiments

### 2.1. Materials preparation and MAO process

Commercial available 2195 Al-Li alloy with dimensions of 20 mm×15 mm×2 mm, was used as a substrate for the MAO process. Its composition is Li- 1.07 wt%, Cu- 3.97 wt%, Mg- 0.4 wt%, Zr-0.15 wt%, Ag-0.25 wt%, Ti-0.10 wt%, and the rest being aluminum. Prior to MAO process, samples were ground using emery abrasive papers up to 2000 grit, followed by ultrasonic cleaning and deoiling with acetone for 10 min, and then washing with deionized water. The MAO process was conducted in a constant current mode for fixed 60 min at different current densities of 2, 4, 6 and 8 A/dm$^2$, respectively. MAO was performed using an alkaline silicate–phosphate composite electrolyte system ($Na_2SiO_3$–$(NaPO_3)_6$–NaOH) as the basic electrolyte. All chemicals were of analytical grade. The composition of the electrolyte is presented in Table 1. The variation of voltage with respect to treatment time was recorded. After the MAO treatment, the specimens were rinsed with deionized water, dried and used for further studies.

The schematic diagram of the experimental device is shown in Figure 1.

**Table 1. The composition of the electrolyte**

| Reagent | Concentration(g/L) |
|---|---|
| $Na_2SiO_3$ | 8 |
| $(NaPO_3)_6$ | 6 |
| NaOH | 0.5 |

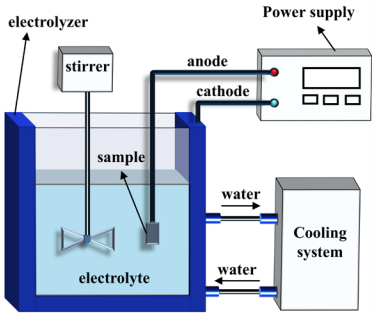


Figure 1. Schematic diagram of the MAO experimental device.

### 2.2. Coating characterization

After micro-arc oxidation, the surface roughness of the samples was measured by surface roughness meter TR200. Five points were selected on both sides, and the average value was recorded. The surface and cross-sectional morphology, thickness, and elemental compositions of the MAO coatings were analyzed by using scanning electron microscopy (SEM, Nova Nano 450) equipped with energy dispersive spectroscopy (EDS, INCA 250X-Max5). To ensure the integrity of the MAO coatings, a Ni-P electroless plating was deposited on samples before

the cross-sectional SEM observations, The basic formula of the Ni-P electroless plating solution is shown in Table 2. The phase analysis of the coatings was utilized by X ray diffractometer (XRD, D8ADVANCE ) with Cu Kα(λ=0.154056 nm) ray, and the scanning range is 10 °~80 °. The Surface Element Composition and Chemical State of Coating was utilized by -ray photoelectron spectroscopy (XPS, Model Axis Supra), and Equipped with a monochromatic Al, Ag dual-anode X-ray source, with a maximum power of 400W.

**Table 2. The basic formula of the Ni-P electroless plating solution**

| Reagent | Concentration(g/L) |
|---|---|
| $NiSO_4$ | 30 |
| $NaH_2PO_2$ | 26 |
| $Na_3C_6H_5O_7$ | 5 |
| $C_4H_6O_4$ | 15 |
| $C_3H_6O_3$ | 15 |
| $C_2H_3O_2Na$ | 20 |

### 2.3. Electrochemical tests

The potentiodynamic polarization tests of the MAO coatings were conducted using an electrochemical workstation of PGSTAT302N, in 3.5 % NaCl solutions at 25 ºC. The electrochemical tests used a conventional three-electrode cell. Meanwhile, the samples with an exposed area of 1 $cm^2$ to the solution were used as the working electrode, a platinum foil acted as the counter electrode, and the saturated calomel electrode (SCE) served as the reference electrode. Before the tests, the electrochemical testing system was stabilized at open circuit potential (OCP) for 30 min. The triplicate experiments were carried out for all samples to ensure reproducibility.

Electrochemical impedance spectroscopy (EIS) of the MAO coatings were performed using a PGSTAT302N electrochemical workstation in 3.5wt% NaCl solution at 25℃. Before the test, the system was stabilized at open circuit potential (OCP) for 30-40 min. All samples were tested in triplicate to ensure the reproducibility of the results.

### 2.4. Wear tests

Using the HT-1000 ball-on-disk friction and wear tester to test the wear resistance of the coatings, the friction pair was selected GCr15 balls with diameter of 4.976 mm, and other wear parameters were load 365 g, friction radius 6 mm, rotational speed 224 r/min, friction time 10 min. The section profile curve is obtained by using the TR200 surface roughness meter and the wear volume V ($mm^3$) is calculated. The wear rate of the coating was calculated according to the formula K=V/SF, in which, the V is the wear volume ($mm^3$), S is the total glide distance (m), and F is the load (N).

## 3. Results and Discussion

### 3.1. Voltage-time curves

The curves of voltage with respect to time under different current densities of 2, 4, 6 and 8 A/$dm^2$ for 60 min during MAO process are shown in Figure 2. It can be seen that the voltage at each current density in the initial 5 min rose rapidly, numerous small bubbles were observed on the surface of Al-Li substrate, These bubbles are mainly $O_2$ produced at the anode and a small amount of water vapor. which is corresponding to the conventional anodic reaction process[17]. After that, the voltage increased slower, and sparks began to emerge and grew on the sample's surface. The higher the current density, the higher voltage at the same MAO treating time. Xiang et al[13] have reported the similar phenomenon. The terminal voltages of the coatings produced under the current densities of 2, 4, 6 and 8 A/$dm^2$ are 468, 503, 522 and 532 V, respectively.

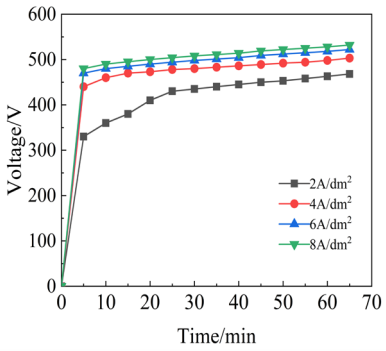


Figure 2. Variation of voltage with time at different current densities

### 3.2. Surface roughness of the coatings

The surface roughness of the MAO coatings under different current densities is shown in Figure 3. As we can see that the surface roughness increased almost linearly with the current density, which is contributed to the presence of more and larger inevitable cavities, open-pores and pancake projection, under higher current density[18]. The roughness values of the coatings under the current densities of 2, 4, 6 and 8 A/$dm^2$ are 0.75, 1.41, 3.25 and 4.01 mm, respectively. Zhang et al[19] also found that in the process of MAO, the size of ceramic micropores and oxide particles increased, which lead to the increases

of the surface roughness.

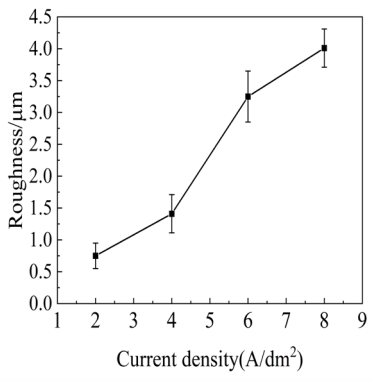


Figure 3. Roughness of the MAO coatings under different current densities.

### 3.3. Surface and Cross Sectional Microstructure of MAO coatings

Figure 4 shows the surface and cross-sectional morphologies of the MAO coatings prepared at different current densities. As can be seen from the diagram, it is evident that the variation in the current density affects the morphology of MAO coatings. As the current density increases, the surface of the coating becomes coarser, rougher and in addition the thickness also increases.

When the current density is 2 A/dm$^2$ (Figure 4(a)), the surface of the coating is relatively uniform, but there are many open-pores. In addition, there exist many micro-cracks on the surface caused by thermal expansion and cold shrinkage during melting and solidification of the molten oxides[20]. The thickness of the MAO coating is about 10 μm from the cross-section morphology in Figure 4(b), and it is uneven, which is also related to the scattered formation of the molten oxides on the surfaces.

When the current density increases to 4 A/dm$^2$, the quantity of the open pores on the surface of the coating are less compared with those in Figure 4(a), and many larger pancake-like molten oxides are formed as shown in Figure 4(c).the pancake-like structures are caused by molten oxide ejected from the discharge channels owing to the rapid solidification under the cooling electrolyte[21]. A similar observation has been reported by Ezhilselvi et al. that the size of the pore increases with an increase in current density with reduced pore density[22], The corresponding cross sectional image exhibits in Figure 4(d), and we can find that the upper layer of the MAO coating becomes relatively denser and well combined with the matrix, but there appear some cavities within the lower part of the MAO coating, which reducing the compactness of the coating.

When the current density increases to 6 A/dm$^2$, large annular volcanic bulges are formed, as shown in Figure 4(e), the surface become rougher. From the cross image in Figure 4(f), it can be seen that there exist obvious thermal cracks, even crossing the coating, which may deteriorate the corrosion resistance of the coating.

Further increasing current density to 8 A/dm$^2$, irregular shape of ceramic oxides appear on the surface of the coating (Figure 4(g)). The discharge energy increases as the current density increases during the MAO process, and the reactions become intense, and more molten oxides are ejected outward and even “splash” occurs[21]. Interestingly, the compactness of the coating, represented in Figure 4(h), is much better than the other three coatings from the cross-sectional morphologies, and the thickness reaches about 60 μm when the current density is 8 A/dm$^2$.

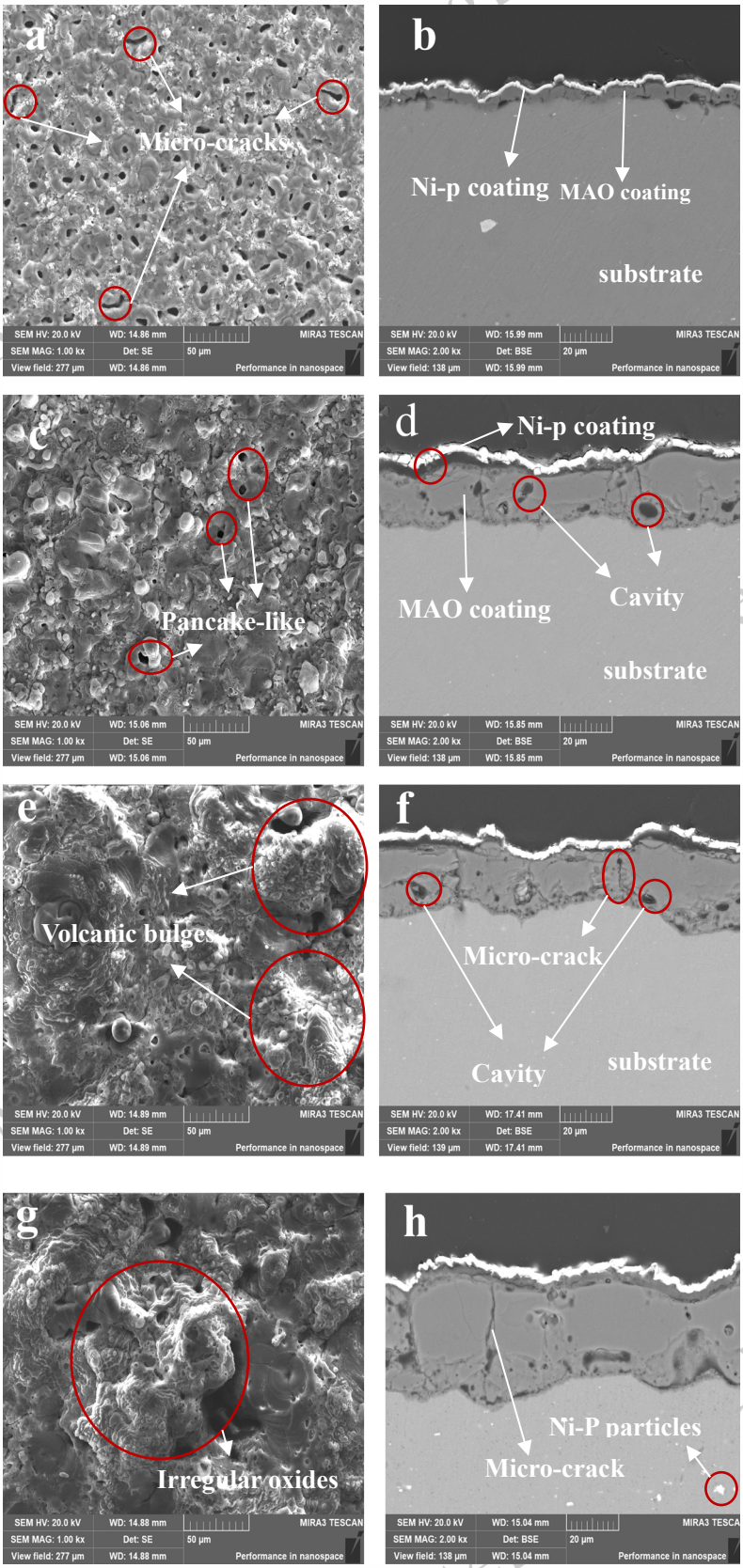


Figure 4. Surface and cross-section morphologies of MAO coatings prepared at current density of 2 A/dm$^2$ (a,b), 4 A/dm$^2$ (c, d), 6 A/dm$^2$ (e, f), 8 A/dm$^2$ (g, h) for 60 min

### 3.4. Elemental Analysis of the MAO coatings

#### 3.4.1. EDS anlysis

Table 3 shows the surface composition of the MAO coatings prepared at different current densities by EDS. It can be seen that the main elements of the coatings are Al, Si, O and a small amount of P, Mg and Na, in which, Al and Mg are mainly from the substrate, Si, P and Na from the electrolyte. In addition, the Si content in the coating increases with the current density. With the increase of current density, the discharge channels become less and larger, and more intense discharging reactions occur, which results in more anions, such as $SiO3^{2-}$, from the electrolyte by adsorption and electrophoresis[22], around the surface and resulted in a higher content in the coating[23]. P and Na also remain on the surface of the coating because of micro-arc oxidation spark sintering.

However, no lithium is detected in the MAO coatings by EDS, and the similar results were also confirmed by XPS for the MAO coatings on Al-Li alloy, and they concluded the lithium did not participate in the reaction during MAO process, QIN also drawn similar conclusions[24]. Considering the poor stability of lithium in an aqueous solution at high temperature, the precipitation of lithium compounds in the substrate resulted in a large number of defects in the anode coating at the beginning[25,26]. On the other hand, the bubble expanded with the growth of the coating and the generated gases were released when the cracks occurred. Then, the increase of thickness and occurrence of dielectric breakdown followed. These effects provoked the enhancement of the electric field and strong micro-discharge, which possessed an immediate impact on the defects in the cross-section of the MAO coatings[27,28], as shown in Figure 4.

#### 3.4.2 XPS analysis

The figure 5 presents the results of X-ray photoelectron spectroscopy (XPS) analysis on the surface of the micro-arc oxidation coating of aluminum-lithium alloy at a current density of 8 A/dm$^2$. The chemical composition of the coating was investigated and elucidated with the binding energy of carbon (284.8 eV) adopted as the reference peak.

Figure 5((b)~(d)) present the high-resolution X-ray photoelectron spectroscopy (XPS) binding energy spectra of Al(2p), O(1s) and Si(2p) for the micro-arc oxidation (MAO) coating on aluminum-lithium alloy, respectively. Specifically, the two characteristic peaks in the Al(2p) spectrum (Figure5(b)) are respectively assigned to the Al–O bonds in γ-$Al_2O_3$ and α-$Al_2O_3$ according to the study reported in Guo[29]; the Si(2p) spectrum is depicted by Figure 5(d) , and this Si corresponds to the silicon in the Si–O bonds of $SiO_2$[30]; the O(1s) spectrum (Figure 5(c)) corresponds to the oxygen species in the Si–O bonds of $SiO_2$ and the Al–O bonds of $Al_2O_3$ respectively.

The XPS analysis results demonstrate that the ceramic coating formed by MAO on the aluminum-lithium alloy surface is mainly composed by $SiO_2$ and $Al_2O_3$. Then, no characteristic peak of lithium was detected in the entire XPS survey, The same results were also obtained in samples 2 A/dm$^2$ to 6 A/dm$^2$. combined with the energy-dispersive X-ray spectroscopy (EDS) results, it can be reasonably concluded that lithium did not participate in the micro-arc oxidation reaction process[24].

**Table 3. Surface EDS analysis results of MAO coatings prepared under different current densities**

| Current (A/dm$^2$) | Elements (wt%) | | | | | |
|---|---|---|---|---|---|---|
| | Al | O | Si | P | Mg | Na |
| 2 | 35.18 | 62.71 | 1.27 | - | 0.85 | - |
| 4 | 32.02 | 63.04 | 4.12 | - | 0.81 | - |
| 6 | 25.36 | 66.06 | 6.82 | 1.02 | 0.74 | - |
| 8 | 20.02 | 63.38 | 13.07 | 1.66 | - | 2.94 |

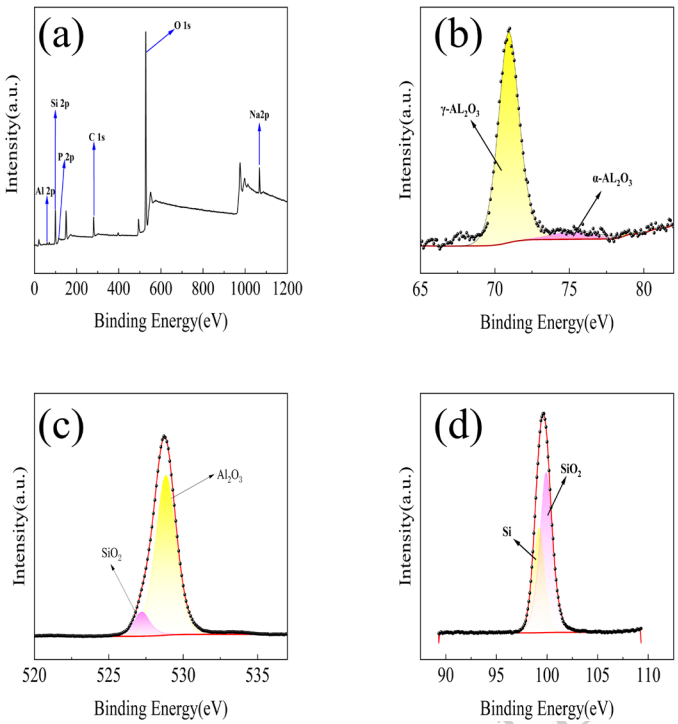


Figure 5. XPS patterns of the MAO coatings prepared at current densities 8 A/dm$^2$ (a) Wide, (b) Al 2p, (c) O 1s (d) Si 2p

### 3.5. Phase composition

For comparison, the XRD patterns of the MAO coatings prepared at current densities of 2 A/dm$^2$ to 8 A/dm$^2$ exhibit in Figure 6. It is found that the main phases of the coatings are γ-$Al_2O_3$ and a small amount α-$Al_2O_3$, and the diffraction peaks of the γ-$Al_2O_3$ are stronger than those of the α-$Al_2O_3$. Similar results are also reported in reference[8,35]. Xiang et al[13] studied the formation mechanism of metastable phase $Al_2O_3$, and found that the nucleation rate of droplet melting γ-$Al_2O_3$ phase is higher than that of α-phase under a large under-cooling. The melted $Al_2O_3$ of the outerlayer of the MAO coating directly contacting with the electrolyte has a large cooling rate, which is beneficial to the formation of γ-$Al_2O_3$ phase. With the increase of current density, the peaks corresponding to α-$Al_2O_3$ are enhanced, indicating more γ-$Al_2O_3$ transformation to α-$Al_2O_3$. And the reason could be attributed to more heat generated at higher current density, and the low thermal conductivity of aluminium oxide[21]. And high temperatures cause the Gibbs free energy of α-$Al_2O_3$ to be significantly lower than that of γ-$Al_2O_3$. The oxide film will spontaneously transform into the more stable α-$Al_2O_3$ crystal phase, and the higher the temperature, the stronger the transformation tendency. This ultimately leads to an increase in the content of α-$Al_2O_3$ in the film layer as the current density increases[21].

For the MAO coatings, the diffraction peaks of Al corresponding to the substrate are detected.

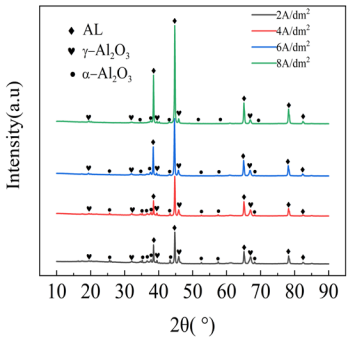


Figure 6. XRD patterns of the MAO coatings prepared at current densities of 2 to 8 A/dm$^2$

### 3.6. Corrosion studies

#### 3.6.1. Potentiodynamic polarization tests

Potentiodynamic polarization curves obtained for the MAO coatings and the substrate alloy are shown in Figure 7, and the results of self-corrosion potential (Eo) and corrosion current density (Io) of each sample are also displayed in Table 4. The bare Al-Li substrate initially shows a steep increase in the anodic potential from about -0.834 V up to the voltage of -0.536 V, indicating a passivation process occurs.

After that, an evident enhanced current density occurs, corresponding to the dissolution process of the formed passivation film. The Eo and Io of the substrate are -0.834 V and 2.359 × $10^{-5}$ A/cm$^2$, respectively. The lower potential and larger corrosion current imply the weak corrosion resistance of the substrate in NaCl solution.

It can also be seen from Figure 7 that with the increase of MAO current density, the self corrosion potential increases, and the corrosion current density decreases, indicating enhanced corrosion resistance of the MAO coatings[36]. When the MAO current density is 2 A/dm$^2$, the surface of the coating is uniform, but it contains many holes, even adjacent holes connected together, which increases the corrosion area and the corrosion resistance of the coating is poor. As the current density increases, the thickness and density of the MAO coatings increase. When the current density is 8 A/dm$^2$, the Eo is -0.536 V, which is shifted positively by about 0.298 V compared with the substrate, and the Io is the lowest, 4.32×$10^{-7}$ A/cm$^2$, in which, the Io is two orders of magnitude smaller than that of the substrate. The corrosion resistance of ceramic layer is mainly related to the thickness of coating and its surface quality[24], When the current density is 8 A/dm$^2$, the surface and cross section of the coatings shown in Figure 4 are more uniform and denser, and the holes are less, which improves its corrosion resistance.

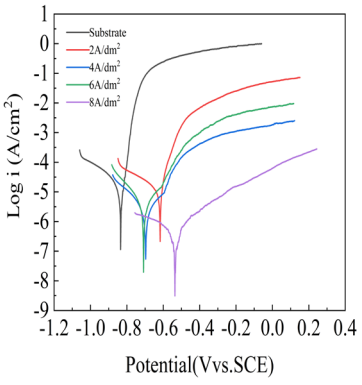


Figure 7. The potentiodynamic polarization curves of the substrate and the MAO coatings prepared at different current densities.

### 3.6.2. Electrochemical Impedance Spectroscopy texts

Electrochemical Impedance Spectroscopy (EIS) can quantitatively evaluate the corrosion resistance of microarc oxidation (MAO) coatings. Figure 8 presents the EIS spectra of MAO ceramic coatings fabricated at different current densities after immersion in 3.5% NaCl solution for 1 h.

As observed from the Nyquist plots in Figure 8(a), the samples treated by MAO at 4 A, 6 A and 8 A only exhibit capacitive arcs in their Nyquist plots, while the sample at 2 A shows both capacitive arc and weak inductive arc. The appearance of inductive arc in the low-frequency region is attributed to the abundant defects in the coating under low current density, which induces the adsorption or desorption behavior of solution ions at the interface[31,32]. A larger radius of the capacitive arc in the Nyquist plot indicates superior corrosion resistance of the MAO coating[33]. It can be seen from the plots that the radius of the capacitive arc increases with the increasing current density, implying that the corrosion resistance is enhanced with rising current density. At a current density of 8 A/dm², the sample exhibits the largest capacitive arc radius among all specimens, indicating that this coating possesses the highest corrosion resistance and the lowest corrosion rate.

From the impedance magnitude-frequency plots in the Bode diagrams (Figure 8(b)), all curves show a rapid decrease in impedance magnitude in the high-frequency region, demonstrating that the capacitive behavior of the coating dominates at high frequencies. In the medium-frequency region, the impedance magnitude increases significantly with decreasing frequency, showing typical capacitive characteristics. In the low-frequency region, the impedance magnitude of the 8 A/dm² sample is the highest, while that of the 2 A/dm² sample is the lowest, which confirms that the protective performance of the coating is improved with increasing current density. At 8 A/dm², the impedance modulus |Z| of the MAO ceramic coating is higher than those of other coatings, indicating that this MAO coating exhibits the highest corrosion resistance and the best protective performance.

In addition, the phase-frequency plots in the Bode diagrams reveal that the MAO coatings have three time constants. The time constant in the high-frequency region corresponds to the loose outer layer, the medium-frequency region corresponds to the dense inner layer, and the low-frequency region corresponds to the electric double layer at the substrate–solution interface. For the 2 A/dm² sample, a significant decrease in phase angle appears in the low-frequency region, which is attributed to the poor coating quality at 2 A/dm², leading to localized corrosion of the substrate. This result corresponds well to the weak inductive arc observed in the Nyquist plots of this group. Moreover, the 8 A/dm² sample shows the

highest phase angle peak, further verifies that its coating exhibits the most remarkable capacitive characteristics and the best structural integrity.

Figure 9 denotes the equivalent circuit of the MAO coating. Table 5 lists the fitting parameters calculated via the ZSimpWin software. $R_p$ and $R_b$ represent the impedance of the outer layer and inner layer of the MAO coating respectively. A higher impedance value corresponds to superior corrosion resistance[34]. It can be seen from the data in Table 5 that the values of $R_p$ and $R_b$ increase with the increasing of current density. When the current density is 8 A/dm², the $R_p$ and $R_b$ values are one order higher than those of the other samples, indicating that the coating fabricated at this current density possesses the optimal compactness and corrosion resistance.

**Table 4. Self-corrosion potential and self-corrosion current densities of the substrate and the MAO coatings prepared under different current densities.**

| Samples produced at current density/(A/dm²) | Eo(V) | Lo (A/cm²) | Rp (Ω*cm²) | Corrosion Rate (mm/a) |
|---|---|---|---|---|
| Substrate | -0.834 | 2.359E-05 | 324.9 | 0.5925 |
| 2 | -0.617 | 1.358E-05 | 165.5 | 1.1632 |
| 4 | -0.696 | 2.064E-06 | 1572.8 | 0.13609 |
| 6 | -0.708 | 2.05E-06 | 1550.4 | 0.11417 |
| 8 | -0.536 | 4.32E-07 | 34804 | 0.005331 |

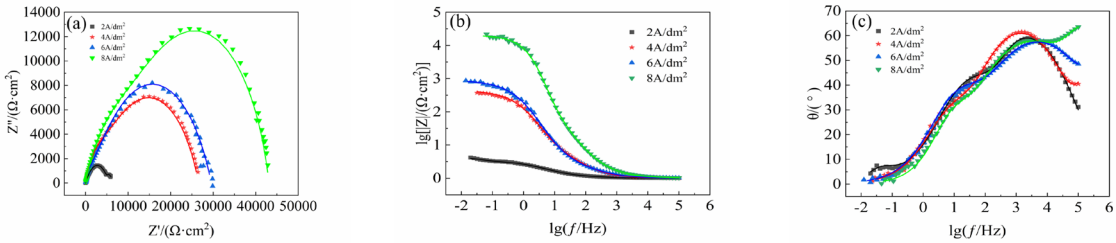


Figure 8. The EIS plots of the MAO coatings prepared at different current densities. (a) Nyquist plots. (b) Bode impedance plots. (c) Bode phase diagrams

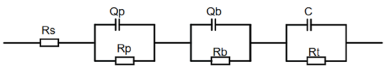


Figure 9. Equivalent circuit diagram of coated specimen

**Table 5. Electrochemical impedance spectroscopy (EIS) fitting data for four samples in 3.5 wt% NaCl electrolyte**

| Sample | 2 A/dm² | 4 A/dm² | 6 A/dm² | 8 A/dm² |
|---|---|---|---|---|
| $R_s(\Omega\cdot cm^2)$ | $7.709\times10^{-5}$ | $4.497\times10^{-5}$ | $4.142\times10^{-5}$ | $9.997\times10^{-3}$ |
| $n_1$ | 0.8858 | 0.6919 | 0.7147 | 0.6866 |
| $R_p(\Omega\cdot cm^2)$ | $2.07\times10^{2}$ | $2.218\times10^{3}$ | $2.382\times10^{3}$ | $1.382\times10^{5}$ |
| $Q_p(\Omega^{-1}\cdot cm^{-2})sn)$ | $5.810\times10^{-6}$ | $6.555\times10^{-6}$ | $2.832\times10^{-6}$ | $1.168\times10^{-6}$ |
| $n_2$ | 0.6635 | 0.7879 | 0.6780 | 0.8124 |
| $R_b(\Omega\cdot cm^2)$ | $5.018\times10^{3}$ | $2.339\times10^{4}$ | $2.714\times10^{4}$ | $2.927\times10^{5}$ |
| $Q_b(\Omega^{-1}\cdot cm^{-2})sn)$ | $2.414\times10^{-5}$ | $1.887\times10^{-6}$ | $5.416\times10^{-6}$ | $2.462\times10^{-6}$ |
| $R_t(\Omega\cdot cm^2)$ | $9.719\times10^{1}$ | $3.925\times10^{1}$ | $2.165\times10^{1}$ | $5.370\times10^{1}$ |
| C | $4.190\times10^{-8}$ | $1.955\times10^{-8}$ | $2.07\times10^{-8}$ | $8.009\times10^{-8}$ |

### 3.7. Wear resistance of film

The friction coefficient curves of the substrate and the MAO coatings prepared at different current densities are shown in Figure 10. It can be seen that when the current density is 2 A/dm$^2$, the friction coefficient curve firstly goes through a "running and stage", and then rises gradually up to 0.9. When the current density is 4 A/dm$^2$, the friction curves underwent a short running-in period and rose fast to about 1.05, and then developed with a small amplitude for 300 s. After that the coefficient tended to stable and increased up to 1.1 in the end of the test. The friction coefficient curves of samples prepared at 6 and 8 A/dm$^2$, were similar to that of 2 A/dm$^2$, but they were more stable and lower, which were 0.45 and 0.50 respectively in the end of the tests。

It can be seen from Figure 10 that the friction coefficients at 2 A/dm² and 4 A/dm² are significantly lower than those at 6 A/dm² and 8 A/dm². This phenomenon can be attributed to the fact that the content of α-$Al_2O_3$ in the coating increases with the elevation of current density. The increased α-$Al_2O_3$ content enhances the coating hardness, which promotes the formation of more wear debris during the friction process. Most of the wear debris exhibit an irregular spherical morphology and act as rolling particles during sliding, thereby reducing the friction coefficient.

Figure 11 shows the surface morphologies of the micro-arc oxidation coating after wear and the wear morphology of the GCr15 small ball used as the friction pair. When the current density is 2 A/dm² and 4 A/dm², the wear tracks are narrow and flat relatively. At high magnification, obvious wear debris and iron filings can be seen as shown in Figure 11 ((b), (e)), and the GCr15 small balls have flat circular wear scars, as shown in Figure 11. ((c), (f)), indicating that the wear mechanism Mainly dominated by abrasive wear. When the micro-arc oxidation current density is further increased to 6 A/dm² and 8 A/dm², there is also a small amount of wear debris, and the GCr15 small balls are worn severely, which also indicates that the wear mechanism is abrasive wear. It can be seen from Figure 11 ((c), (f), (i), (l)) that the wear area of the GCr15 small balls increases with the increasing of the current density. This is because both the hardness and the thickness of the micro-arc oxidation coating increase[37]with the current density increasing, which leads to the gradual aggravation of the GCr15 small balls wear.

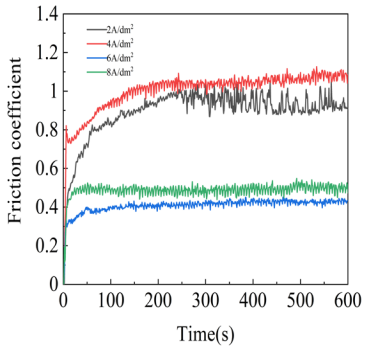


Figure 10. The friction coefficient curves of the substrate and the MAO coatings.

The wear rate of the MAO coatings is illustrated in Figure 12. It can be seen that, with the current density increasing, the wear rate decreased. When the current density is 8 A/dm$^2$, the wear rate is $0.1355\times10^{-3}$ mm$^3$/N·m and minimum, showing the best wear resistance. Similar results were also reported by Xin et al.[38]and Yang et al.[39]

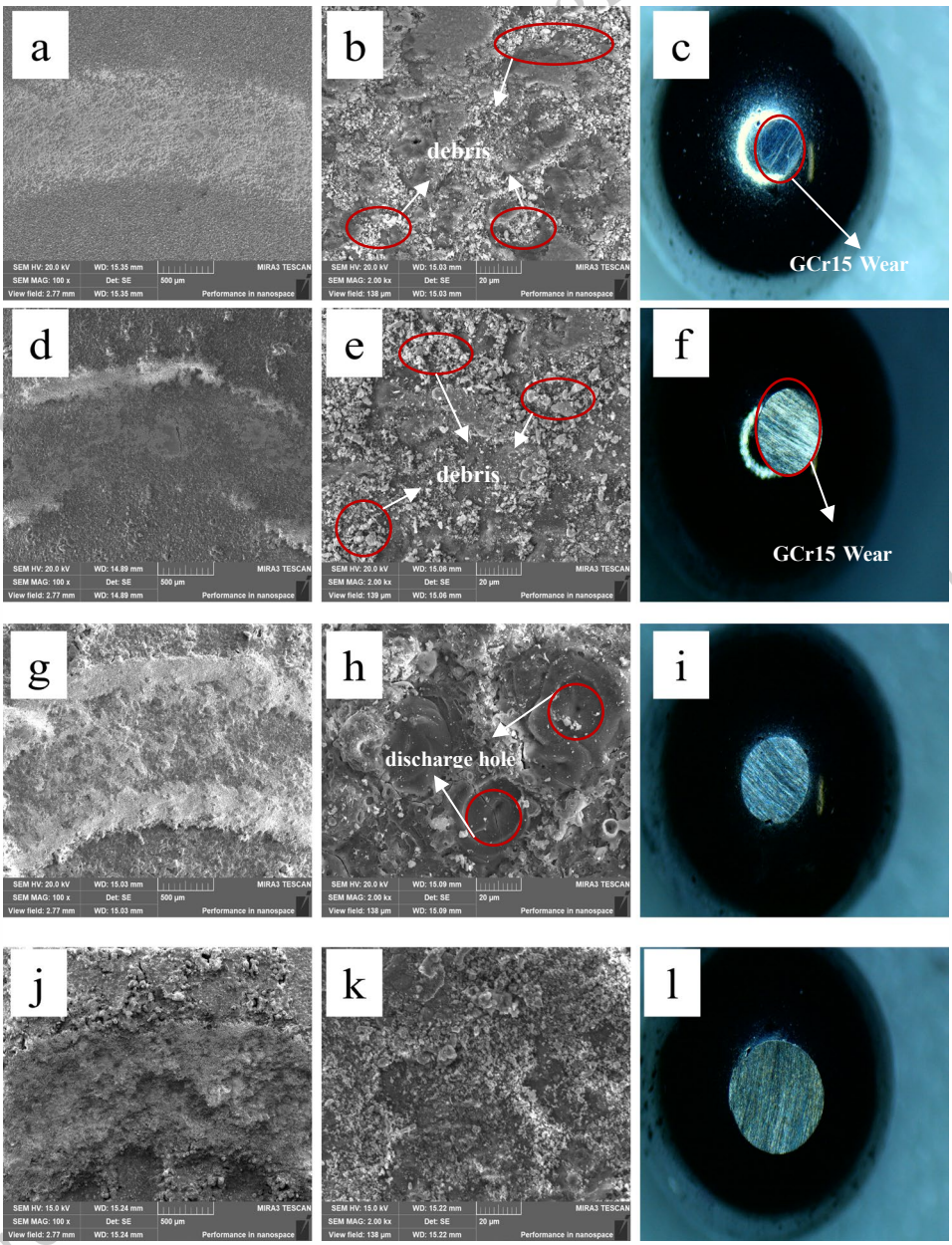


Figure 11. Wear morphology of micro-arc oxide coatings prepared under different current densities of 2 A/dm$^2$ (a,b,c), 4 A/dm$^2$ (d,e,f), 6 A/dm$^2$ (g,h,i), 8 A/dm$^2$ (j,k,l)

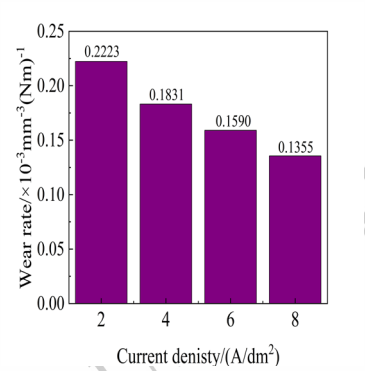


Figure 12. Wear rate of oxide films prepared under different current densities.

## 4. Conclusion

1) The MAO coatings prepared on 2195 Al-Li alloy through DC steady current mode at different current densities ranged from 2 to 8 A/dm$^2$, are uniform and mainly composed of γ-$Al_2O_3$ and a small amount of α-$Al_2O_3$.
2) With the increase of current density, the terminal voltages, roughness and thickness of the MAO coatings increase remarkably. The corrosion resistance of contings increase with the current density. When the current density is 8 A/dm$^2$, the corrosion potential is -0.536 V, which is shifted positively by about 0.298V compared with the substrate, and the corrosion current is the lowest, $4.32\times10^{-7}$ A/cm$^2$, which is two orders of magnitude smaller than that of the substrate.
3) The wear resistance of the MAO coatings increases with the current density. And the wear mechanism is abrasive wear. When the current density is 8 A/dm$^2$, the MAO coatings show the best wear resistance with a minimum wear rate of $0.1355\times10^{-3}$ mm$^3$/N·m.

## References


1. Zhang Wenxin, Zhang Xiankun, Shi Lei, Li Shengli, Jiang Yuanning, Wu Chuansong.Rare Metal Materialsand Engineering.[J],2025,54(2):311~318.
2. Chunyan D, Hui Z, Zhiyong D et al.Materials Letters[J],2019,236:723-726.
3. Xu J L, Xiao X F, Mei D D et al.Surface and Coatings Technology[J],2017,309:621-627.
4. Nan Xiang, Song GuoRen, Jian Zhao et al.Transactions of Nonferrous Metals Society of China[J],2015,25(10):3323-3328.
5. hangkai Wang, Honghua Hu, Shan Du, Bo Cheng, Yanyan Pan, Hailin Lu et al.Materials Chemistry and Physics[J],2024,328:130031-130031
6. Yulin Zhang, FeiChen, Youzhang et al. Materials Letters[J],2021,303:130506.
7. He J, Cai Q Z, Luo H H et al.Journal of Alloys and Compounds[J],2009,471(1):395-399.
8. D L Yu, B Jiang, X Qi et al.Materials Today Communications[J],2024,40:109868.
9. Zhanshuai Fan, Qing Liu, Nan Tu, Jian Chen, Hailin Lu et al.Tribology International[J],2023,190:109048.
10. Hussein R O, Northwood D O, Nie X et al.Surface and Coatings Technology[J],2013,237(25):357-368.
11. Mingjin Wu, Feng Jiang et al.Materials Characterization[J],2024,215:114218.
12. Kalkanci H; Kurnaz S C et al.Surface and Coatings Technology[J],2008,203(1-2):15-22.
13. Xiang N, Song R, Zhuang J et al.Transactions of Nonferrous Metals Society of China[J],2016,26(3):806-813.
14. Lan Xinyue, Wang Ping, Gong Zeyu, Luo Xu, Zheng Youping, Deng Bowen.Rare Metal Materials and Engineering.[J],2024,53(4):954~962.
15. Zhenhua Liu, Hailin Lu, Ziyue Zhao, Zhiqiang Zhu, Suobin Li.Applied Surface Science[J],2025,679(15):161067.
16. Sun Fengyu, Yang Zhao, Hu Jie, Gong Yunbai, Wang Ping, Luo Qiming, Zhu Manlan.Rare Metal Materials and Engineering.[J],2025,54(1):76~83.
17. Qixing Xia, Xiang Li, Zhongping Yao, Zhaohua Jiang.Surface and Coatings Technology[J],2021,409:126874.
18. Ye Wang, Danhua Lu, Guolong Wu et al.Surface and Coatings Technology[J],2020,393:125815.
19. Zang Y, Wu Y, Chen D et al.Surface and Coatings Technology[J],2017,321:236-246.
20. Salih Durdu, Aylin Aytaç, Metin Usta.Journal of Alloys and Compounds[J],2011,509(34):8601–8606.
21. Peng Z, Xu H, Liu S, Qi Y, Liang J.Materials[J],2021,14(14):4037
22. V. Ezhilselvi, J. Nithin, J.N. Balaraju, S. Subramanian.Surface and Coatings Technology[J],2016,288: 221–229
23. Yupeng Guo, Zhenguo Wei, Xiaofeng Lu, et al. Surface and Coatings Technology[J],2021,426:127765
24. Ying Qin, Guo-hua Wu, Andrej Atrens et al.Transactions of Nonferrous Metals Society of China[J],2021,31(4):913−924.
25. Hussein R O, Nie X, Northwood D O, Yerokhin A, Matthews A.Journal of Physics D: Applied Physics [J], 2010, 43(10):105203.
26. Hussein R O, Nie X, Northwood D O.Electrochimica Acta[J],2013,112:111−119.

27. Yuanhang Yang, Gang Feng, Yanhong Gu et al.Anti-Corrosion Methods and Materials[J],2021,68(5):404-412.
28. Ma Yan-long, Zhou Xun-xiu, Thompson G E er al.Electrochimica Acta[J],2012,80:148−159.
29. Yupeng Guo, Zhenguo Wei, Xiaofeng Lu, Ruiwen Xu, Yuyang Fei, Da Chen, Haoran Ding.Surface and Coatings Technology[J],2021,426(25):127765
30. Chunyan Du, Hui Zhao, Zhiyong Dai, Zhiyu Tian, Jinchuan Wang, Zhen Wang.Materials Letters[J],2019,236:723-726
31. Gnedenkov A, Lamaka S, Sinebryukhov S, et al.Corrosion Science[J],2021,182:109254.
32. Jiang X, Guo R, Jiang S.Journal of Magnesium and Alloys[J],2016,4(3):230-241.
33. Tang M, Li W, Liu H, et al. Current Applied Physics[J],2012,12(5):1259-1265.
34. Chen Y, Li J, Yang W, et al. Applied Surface Science[J],2019,493:1224-1235
35. Dehnavi V, Liu XY, Luan BL, Shoesmith DW, Rohani S.Surface and Coatings Technology[J],2014,251:106-114.
36. Ma Y, Zhou X, Huang W et al.Corrosion Engineering, Science and Technology[J],2015,50(6):420-424.
37. Dos S S C, Antunes M L P, Dalla V L V O et al. Journal of Cleaner Production[J],2019,222:584-592.
38. Xin Yang, Wan-lin Wang, Wen-jun Ma et al.ransactions of Nonferrous Metals Society of China[J],2020,30(8):2132-2142
39. Yang Mei, Tang Ning, Chen Jin et al. Rare Metal Materials and Engineering[J],2020,49(2):0404-0411.

# 电流密度对 2195 铝锂合金在硅磷酸盐电解液中微弧氧化涂层的微观结构、耐腐蚀性及耐磨性的影响

靳宗翰，冯长杰，张宇迪，吴鸿，王赫男

*School of Materials Science and Engineering, Shenyang Aerospace University, Shenyang110136, China;*

沈阳航空航天大学，材料科学与工程学院，中国，沈阳 110136

**摘 要：** 在硅酸盐 - 磷酸盐电解液中，采用微弧氧化（MAO）技术在 2195 铝锂合金表面制备陶瓷涂层，研究了不同电流密度（2-8 A/dm²）对涂层微观结构、耐蚀性和耐磨性的影响。通过扫描电子显微镜（SEM）、能谱仪（EDS）、X 射线衍射仪（XRD）、X 射线光电子能谱仪（XPS）和表面粗糙度仪分析了微弧氧化涂层的表面及截面形貌、成分和粗糙度。结果表明，随着电流密度的增大，微弧氧化涂层的粗糙度和厚度均增加。该涂层主要由 γ-$Al_2O_3$组成，并含有少量 α-$Al_2O_3$。在最大电流密度下制备的微弧氧化涂层最为致密。动电位极化测试表明，涂层的耐蚀性随电流密度的增大而提高。当电流密度为 8 A/dm² 时，微弧氧化涂层的耐蚀性最佳，其腐蚀电位为 - 0.536 V，腐蚀电流密度为 $4.32\times10^{-7}$ A/cm²，较基体降低了两个数量级。电化学阻抗谱（EIS）结果显示，电流密度为 8 A/dm² 时，试样的容抗弧半径最大，且在低频区具有最高的阻抗值。微弧氧化涂层的耐磨性随电流密度的增大而提高。当电流密度为 2 A/dm² 时，磨损机制主要为磨粒磨损；进一步增大电流密度后，磨损机制仍为磨粒磨损。在 8 A/dm² 下制备的微弧氧化涂层耐磨性最佳，磨损率为 $0.1355\times10^{-3}$ mm³/（N · m）。

**关键词：** 铝锂合金; 微弧氧化; 微观结构; 耐腐蚀性; 耐磨性

---

**基金项目：** 辽宁省“兴辽英才计划”（项目编号：XLYC 2002031）

**作者介绍：** 靳宗翰，男，硕士，沈阳航空航天大学材料科学与工程学院，辽宁 沈阳 110136，E-mail: 13361359636@126.com。

**通讯作者：** 冯长杰，男，博士，教授，沈阳航空航天大学材料科学与工程学院，辽宁 沈阳 110136， E-mail: chjfengniat@126.com。